Aerospace Science and Technology 120 (2022) 107245

Contents lists available at ScienceDirect

Aerospace Science and Technology

www.elsevier.com/locate/aescte

Control of centrally-powered variable pitch propeller quadcopters subject to propeller faults

Zhikun Wang [a,b], Roderich Groß [a], Shiyu Zhao [b,*]

[a] Department of Automatic Control and Systems Engineering, The University of Sheffield, United Kingdom
[b] School of Engineering, Westlake University, China

ARTICLE INFO

Article history:
Received 25 May 2021
Received in revised form 1 November 2021
Accepted 24 November 2021
Available online 29 November 2021
Communicated by Xiande Fang

Keywords:
Variable pitch propeller quadcopter
Flight control
Fault control

ABSTRACT

Research into variable pitch propeller (VPP) quadcopters has seen a marked increase in recent years which is due to their enhanced dynamic capabilities compared to conventional fixed pitch propeller quadcopters. Adding actuators to control the pitch angles of the propellers increases the mechanical complexity and hence may increase the risk of faults. In this paper, the flight control of a centrally-powered VPP quadcopter in the presence of a propeller fault is studied. This problem has not been studied in the literature. In this paper firstly the balance trajectory is analysed. The uncontrollable mode is identified next. Finally, a linear controller is proposed. It is shown that the yaw angle and angular velocity become uncontrollable in the presence of a VPP fault, yet the quadcopter can still accurately track a desired trajectory. It is also discovered that the quadcopter exhibits different and favourable behaviour, such as slow self-spinning speed. The relationship under certain parameter conditions is analysed and the parameter conditions that lead to zero self-spinning are identified. Our analysis could contribute to the development of high-performance quadcopters that are both agile and robust with respect to faults. Simulation results are presented to verify the theoretical findings.

1. Introduction

Recent years have witnessed the rapid development of commercial micro unmanned aerial vehicles (UAVs) across the world. Due to the simplicity and low cost of their mechanical and dynamical systems, quadcopter UAVs have been successfully applied in many domains [1,2]. In the future, quadcopter UAVs are expected to be routinely utilised in common, day-to-day tasks, such as parcel delivery or passenger transportation [3]. Many of these tasks are safety-critical and require UAVs to achieve high flight performance in terms of both agility and safety [4–7].

Variable pitch propeller (VPP) quadcopters are generalised variants of fixed pitch propeller quadcopters. They have attracted increasing attention in recent years [8–11]. One advantage of them is that they have the same overall control structure as conventional fixed pitch propeller quadcopters. Hence, they inherit the simplicity of the overall dynamical structure from fixed pitch propeller quadcopters, and therefore have the potential to be widely applied in practice.

The difference between a VPP and a fixed pitch propeller is that an actuator is used to control the pitch angle. Adding such actuators remarkably enhances the flight capability of a quadcopter in a number of ways. Firstly, a VPP can generate forces in either upward or downward directions. This novel property brings benefits to the flight control performance. For example, a VPP quadcopter will be able to fly upside down steadily, which is not possible to achieve with a conventional quadcopter. It also enables VPP quadcopters to recover swiftly from largely disturbed attitudes back to stable hovering conditions, which is important considering the safety of the system. Secondly, as the thrust magnitude of a VPP is controlled by adjusting the pitch angle, the control bandwidth is much higher than with spinning speed control, the method used by conventional fixed pitch propellers to adjust their thrust magnitude. The drawback of adding actuators to adjust pitch angles is that it increases the mechanical complexity and hence may increase the fault rate. It is therefore important to study flight control of VPP quadcopters in the presence of actuator faults.

Although fault-tolerant control of quadcopters has been studied extensively [12–15], the case of VPP quadcopters remains largely unexplored. Two recent works [11,16] have studied control of separately-powered VPP (SVPP) quadcopters with one faulty propeller. If one VPP is faulty, an SVPP quadcopter still has six in-

* Corresponding author.
E-mail address: zhaoshiyu@westlake.edu.cn (S. Zhao).

https://doi.org/10.1016/j.ast.2021.107245
1270-9638/

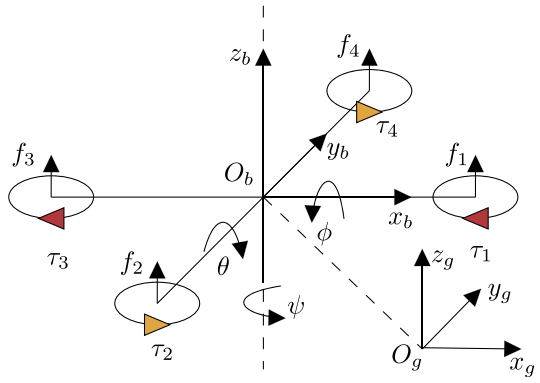

Fig. 1. The schematic diagram of a quadcopter.

dependent control inputs (i.e., three motor spinning speeds and three pitch angles), and the entire system remains controllable. By contrast, our present work addresses the control of centrally-powered variable pitch propeller (CVPP) quadcopters. For a CVPP quadcopter, all propellers spin at the same constant speed; they are driven by the same motor located at the centre of the body [17,18]. If one propeller is faulty, there would only be three independent control inputs, and the entire system becomes uncontrollable and hence more challenging to handle than the SVPP case.

The main theoretical contribution of this paper is to discover that a CVPP quadcopter can exhibit different but favourable behaviour such as a slow self-spinning speed in the presence of a propeller fault. The relationship between the self-spinning speed and the parameter conditions is analysed and the parameter conditions that lead to zero self-spinning in the presence of one propeller fault are identified. Such a discovery is favourably surprising. The theoretical findings are supported by analysing the equilibrium trajectory, identifying the uncontrollable modes, proposing an H_∞ controller and simulating it in two validation experiments. The aforementioned properties make CVPP quadcopters an attractive platform and may stimulate further research and application in the future.

2. Problem setup

Consider a CVPP quadcopter with a "plus" configuration where propellers 1 and 3 rotate clockwise and propellers 2 and 4 rotate counter-clockwise as shown in Fig. 1. There are two coordinate frames: a global inertial frame and a body frame. The origin of the body frame expressed in the global frame is $[x, y, z]^T$. The yaw-pitch-roll angles $[\phi, \theta, \psi]^T$ represent the rotational transformation from the body frame to the global frame. The angular rate of the quadcopter expressed in the body frame is $[p, q, r]^T$. The linear speed of the quadcopter in the global frame is $[u, v, w]^T$. The whole state vector of the quadcopter is $\mathbf{x} = \left[x, y, z, \phi, \theta, \psi, p, q, r, u, v, w\right]^T$.

The translational and rotational air resistance $\mathbf{F}_D$ and $\boldsymbol{\tau}_D$, that oppose the motion of an aircraft, are given by

$$\mathbf{F}_D = -k_\beta \begin{bmatrix} u|u| \\ v|v| \\ w|w| \end{bmatrix}, \quad \boldsymbol{\tau}_D = -k_\gamma \begin{bmatrix} p|p| \\ q|q| \\ r|r| \end{bmatrix},$$

where k_β and k_γ are translational and rotational air resistance coefficients, respectively [19–21].

Overall, the dynamic model for a CVPP quadcopter is identical to that of a fixed pitch propeller quadcopter. The translational motion of the quadcopter is given by [22]

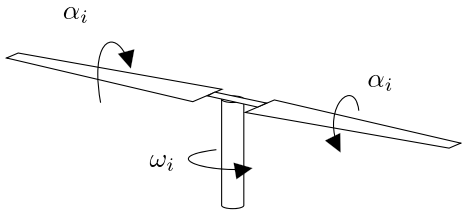

Fig. 2. The schematic structure diagram of a counter-clockwise rotating VPP.

$$\begin{bmatrix} \dot{x} \\ \dot{y} \\ \dot{z} \\ \dot{u} \\ \dot{v} \\ \dot{w} \end{bmatrix} = \begin{bmatrix} u \\ v \\ w \\ \frac{(\cos\psi\sin\theta\cos\phi+\sin\psi\sin\phi)u_1-k_\beta u|u|}{m} \\ \frac{(\sin\psi\sin\theta\cos\phi-\cos\psi\sin\phi)u_1-k_\beta v|v|}{m} \\ \frac{(\cos\theta\cos\phi)u_1-k_\beta w|w|}{m} - g \end{bmatrix}, \tag{1}$$

and the rotational motion of the quadcopter is described by

$$\begin{bmatrix} \dot{\phi} \\ \dot{\theta} \\ \dot{\psi} \\ \dot{p} \\ \dot{q} \\ \dot{r} \end{bmatrix} = \begin{bmatrix} p + q\sin\phi\tan\theta + r\cos\phi\tan\theta \\ q\cos\phi - r\sin\phi \\ q\sin\phi\sec\theta + r\cos\phi\sec\theta \\ qr\frac{I_z-I_y}{I_x} + u_3\frac{l}{I_x} - p|p|\frac{k_\gamma}{I_x} \\ rp\frac{I_x-I_z}{I_y} + u_2\frac{l}{I_y} - q|q|\frac{k_\gamma}{I_y} \\ u_4\frac{l}{I_z} - r|r|\frac{k_\gamma}{I_z} \end{bmatrix}, \tag{2}$$

where I_x, I_y, and I_z are the moments of inertia, l is the half length of the diagonal wheelbase of the CVPP quadcopter, m is the mass of the CVPP quadcopter, and g is the gravitational acceleration constant. The inputs u_1, u_2, u_3, u_4 in (1) and (2) are given by

$$\mathbf{u} = \begin{bmatrix} u_1 \\ u_2 \\ u_3 \\ u_4 \end{bmatrix} = \begin{bmatrix} f_1 + f_2 + f_3 + f_4 \\ f_3 - f_1 \\ f_4 - f_2 \\ -\tau_1 + \tau_2 - \tau_3 + \tau_4 \end{bmatrix}, \tag{3}$$

where f_1, f_2, f_3, f_4 and $\tau_1, \tau_2, \tau_3, \tau_4$ are the thrust forces and torques generated by the four rotors, respectively. The element-wise form of the model in (1) and (2) could be written in a matrix-vector form as $\dot{\mathbf{x}} = \mathbf{f}(\mathbf{x}, \mathbf{u})$, where $\mathbf{f}$ represents the right-hand side of (1) and (2).

The key difference between VPP and conventional fixed pitch propeller quadcopters is the model of their thrust forces and torques. In particular, the force and torque generated by a VPP are, respectively,

$$\begin{aligned} f_i &= k_1\omega_i^2\alpha_i, \\ \tau_i &= k_2\omega_i^2 + k_3\omega_i^2\alpha_i^2 + k_4\omega_i\alpha_i, \end{aligned} \tag{4}$$

where ω_i is the spinning rate of propeller i, α_i is the pitch angle of the propeller, and k_1, k_2, k_3 and k_4 are drag coefficients [23]. Fig. 2 illustrates the structure of a VPP.

For a CVPP quadcopter the spinning rates of the four propellers are identical. That is, it has $\omega_i = \omega_0$ for all i. To simplify (4), the drag coefficients are combined with the fixed spinning speed which gives $b_1 = k_1\omega_0^2$, $b_2 = k_2\omega_0^2$, $b_3 = k_3\omega_0^2$, and $b_4 = k_4\omega_0$, where (4) becomes

$$\begin{aligned} f_i &= b_1\alpha_i, \\ \tau_i &= b_2 + b_3\alpha_i^2 + b_4\alpha_i. \end{aligned} \tag{5}$$

It can be seen that f_i is linearly proportional to α_i whereas τ_i is a second-order polynomial of α_i.

Consider the scenario where the pitch angle of propeller 1 becomes stuck at a constant value c. Substituting $\alpha_1 = c$ and (5) to (3) gives

$$u_1 = b_1(c + \alpha_2 + \alpha_3 + \alpha_4), \tag{6}$$

$$u_2 = b_1(\alpha_3 - c), \tag{7}$$

$$u_3 = b_1(\alpha_4 - \alpha_2), \tag{8}$$

$$u_4 = b_3(-c^2 + \alpha_2^2 - \alpha_3^2 + \alpha_4^2) + b_4(-c + \alpha_2 - \alpha_3 + \alpha_4). \tag{9}$$

In this case, u_1, u_2, u_3, u_4 are not independent anymore since there are merely three degree of freedoms.

3. Equilibrium analysis

In this section, the equilibrium of the nonlinear faulty system is identified firstly, and then a quantitative study of the equilibrium points which reveals some interesting and unique properties of CVPP quadcopters is presented.

3.1. Equilibrium trajectory

To find an equilibrium point for the quadcopter dynamic equation, let the right parts of equations (1) and (2) equal 0. This gives $u_1^* = mg$, $u_2^* = 0$, $u_3^* = 0$, and $u_4^* = 0$. Moreover, according to the assumption that propeller 1 becomes stuck at a constant angle $\alpha_1 = c$, we can substitute these requirements and constrains into (6)-(9) which gives

$$\begin{aligned} mg &= b_1(c + \alpha_2 + \alpha_3 + \alpha_4), \\ 0 &= b_1(\alpha_3 - c), \\ 0 &= b_1(\alpha_4 - \alpha_2), \\ 0 &= b_3(-c^2 + \alpha_2^2 - \alpha_3^2 + \alpha_4^2) + b_4(-c + \alpha_2 - \alpha_3 + \alpha_4). \end{aligned}$$

This is a system with 4 equations and 3 unknowns, which cannot be solved. Only 3 constraint equations can be satisfied in the system, and one cannot. Compared with the loss of attitude, pitch and roll control which is likely to cause the quadcopter to crash, the loss of yaw control seems acceptable. Therefore, we have $u_1^* = mg$, $u_2^* = 0$, and $u_3^* = 0$, substituting which into (6)-(8) gives

$$\alpha_2^* = \alpha_4^* = \frac{mg}{2b_1} - c, \quad \alpha_3^* = c. \tag{10}$$

Furthermore, substituting (10) into (9) yields

$$u_4^* = 2b_3\left(\alpha_4^2 - c^2\right) + 2b_4(\alpha_4 - c). \tag{11}$$

Moreover, substituting $\dot{r}^* = 0$ to (2) gives

$$r^* = sgn(u_4^*)\sqrt{\frac{|u_4^*|l}{k_\gamma}}, \tag{12}$$

where sgn$(\cdot)$ denotes the sign function. When $\alpha_2^* = \alpha_4^* \neq c$, (11) gives $u_4^* \neq 0$ and $r^* \neq 0$ which indicates that the CVPP quadcopter would not be able to remain at any static equilibrium point but can follow a state trajectory with constant self-spinning speed.

In particular, consider a state trajectory

$$\begin{aligned} \mathbf{x}^*(t) &= \left[x^*, y^*, z^*, \phi^*, \theta^*, \psi^*(t), p^*, q^*, r^*, u^*, v^*, w^*\right]^T \\ &= \left[x^*, y^*, z^*, 0, 0, \psi^*(t), 0, 0, r^*, 0, 0, 0\right]^T, \end{aligned}$$

Table 1
CVPP quadcopter parameters.

Parameters	Name	Value	Unit
Mass	m	1	kg
Gravitational acceleration	g	10	m/s^2
Inertia about x_b, y_b	I_x,I_y	0.125	$kg \cdot m^2$
Inertia about z_b	I_z	0.25	$kg \cdot m^2$
Arm length	l	1	m
Force coefficient	k_1	$2.86 \cdot 10^{-5}$	-
Torque coefficient	k_2	$1 \cdot 10^{-8}$	-
	k_3	$6.56 \cdot 10^{-7}$	-
	k_4	$2.29 \cdot 10^{-5}$	-
Pitch angle limit	α_{sat}	0.3142	rad
Pitch angle rate limit	d_α	11.62	rad/s
Motor speed limit	$\omega_{\max}$	1047.19	rad/s
Motor speed rate limit	d_ω	6047	rad/s^2
Linear resistance coefficient	k_β	0.01	$N \cdot s/m$
Rotation resistance coefficient	k_γ	0.05	$N \cdot s \cdot m$

where x^*, y^*, z^*, r^* are constant values and $\psi^*(t) = r^*t + \psi_0^*$. The state trajectory $\mathbf{x}^*(t)$ corresponds to the case where the yaw angle $\psi^*(t)$ varies at a constant value r^* while all the other states are constant.

Along $\mathbf{x}^*(t)$, we have $\dot{u}^*$, $\dot{v}^*$, $\dot{w}^*$, $\dot{p}^*$, and $\dot{q}^*$ equal to 0.

In terms of control inputs, since there are only three functional servos, we choose the three pitch angles as the new inputs. Along the equilibrium trajectory, we have

$$\begin{aligned} \mathbf{u}_F^* &= \left[\alpha_2^*, \alpha_3^*, \alpha_4^*\right]^T \\ &= \left[\frac{mg}{2b_1} - c, c, \frac{mg}{2b_1} - c\right]^T, \end{aligned}$$

where the subscript F represents 'fault'.

3.2. Quantitative study of the equilibrium

Along the equilibrium trajectory, the quadcopter would rotate at a constant rate of r^* as given in (12). It is of great interest to see the specific values of r^*, especially whether r^* could be zero.

Substituting $b_1 = k_1\omega_0^2$, $b_3 = k_3\omega_0^2$, and $b_4 = k_4\omega_0$ into (11) gives

$$u_4^* = \frac{k_3 m^2 g^2}{2k_1^2\omega_0^2} + \frac{k_4 mg}{k_1\omega_0} - \left(\frac{2mgk_3}{k_1} + 4k_4\omega_0\right)c, \tag{13}$$

substituting which into (12) yields

$$r^* = \sqrt{\left[\frac{k_3 m^2 g^2}{2k_1^2\omega_0^2} + \frac{k_4 mg}{k_1\omega_0} - \left(\frac{2mgk_3}{k_1} + 4k_4\omega_0\right)c\right]\frac{l}{k_\gamma}}. \tag{14}$$

The parameters could be selected according to [23], as shown in Table 1.

Although it is assumed that ω_0 is fixed in each control process, we would like to analyse the impact of different values of ω_0 on r^*. First, suppose that the physically achievable interval of ω_0 is $[0, \omega_{\max}]$. Second, since ω_0 must satisfy (10), it follows that

$$\omega_0 = \sqrt{\frac{mg}{2k_1(\alpha_2^* + c)}}. \tag{15}$$

Suppose the physically achievable pitch angle is saturated by $[-\alpha_{\text{sat}}, \alpha_{\text{sat}}]$, where $\alpha_{\text{sat}} = 0.314$ rad following [9]. Since $\alpha_2^* > -c$ by (10), we know $\alpha_2 \in (-c, \alpha_{\text{sat}}]$. It then follows from (15) that $\omega_0 \in \Omega_2 = \left[\sqrt{\frac{mg}{2k_1(\alpha_{\text{sat}}+c)}}, +\infty\right)$. Thus, ω_0 must satisfy

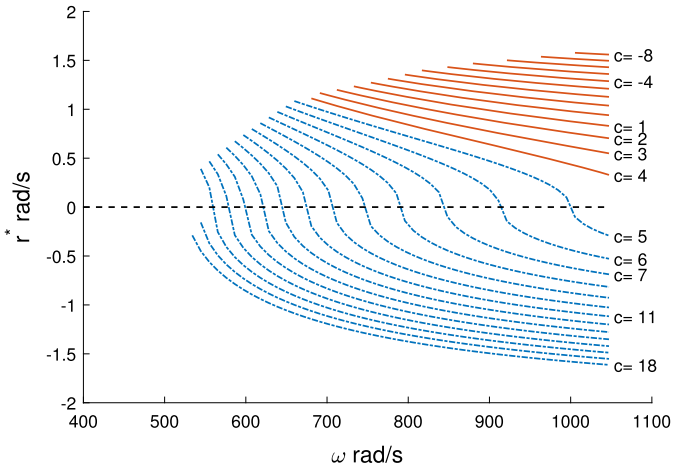

Fig. 3. The relationship between a VPP quadcopter's self rotation speed r^* and its centrally-controlled propeller spinning speed w_0, as expressed by (14). Shown for different angles c (in degree) at which faulty propeller 1 became stuck. The interval of ω_0 for each curve is given in (16). (For interpretation of the colours in the figure(s), the reader is referred to the web version of this article.)

$$\omega_0 \in \Omega_1 \cap \Omega_2 = \left[\sqrt{\frac{mg}{2k_1(\alpha_{\text{sat}}+c)}}, \omega_{\max}\right] := [\omega_{\min}, \omega_{\max}]. \tag{16}$$

To determine the admissible interval of c, it is notable that (16) implies

$$0 \le \frac{mg}{2k_1(\alpha_{\text{sat}}+c)} \le \omega_{\max}^2,$$

which gives $c \ge \frac{mg}{2k_1\omega_{\max}^2} - \alpha_{\text{sat}}$. Furthermore, since $c \in [-\alpha_{\text{sat}}, \alpha_{\text{sat}}]$, it follows that

$$c_{\min} := \frac{mg}{2k_1\omega_{\max}^2} - \alpha_{\text{sat}} \le c \le \alpha_{\text{sat}}. \tag{17}$$

The interpretation is that, if the faulty propeller became stuck at the angle $c < c_{\min}$, then (15) could not hold and hence the system could not reach the equilibrium point.

When c varies in $[c_{\min}, \alpha_{\text{sat}}]$, the values of r^* against w_0 are shown in Fig. 3. This figure suggests two important properties. First, the values of r^* for different c are within a small interval: $[-0.13, 0.13]$ rad/s. As a result, the quadcopter self-rotates slowly at the equilibrium. Second, surprisingly, w_0 can be tuned to make $r^* = 0$ for certain c (see blue dotted curves in Fig. 3). In this case, a CVPP quadcopter could hover steadily without self-rotation in the presence of a propeller fault.

To examine the case of $r^* = 0$ more closely, substituting $r^* = 0$ into (14) gives

$$\frac{k_3 m^2 g^2}{2k_1^2\omega_0^2} + \frac{k_4 mg}{k_1\omega_0} = \left(\frac{2mgk_3}{k_1} + 4k_4\omega_0\right)c, \tag{18}$$

which implies

$$c = \frac{mg}{4k_1\omega_0^2} \tag{19}$$

or equivalently

$$\omega_0^* = \sqrt{\frac{mg}{4k_1 c}}. \tag{20}$$

Therefore, given a specific value of ω_0, if angle c at which propeller 1 became stuck satisfies (19), then it gives $r^* = 0$. On the other hand, given a specific value of c, if ω_0 satisfies (20), then it gives $r^* = 0$.

Since $c \in [c_{\min}, \alpha_{\text{sat}}]$ and $\omega_0 \in [\omega_{\min}, \omega_{\max}]$, examining under what conditions (19) holds is needed. Since $\omega_0 \in [\omega_{\min}, \omega_{\max}]$, it follows from (19) that

$$c = \frac{mg}{4k_1\omega_0^2} \le \frac{mg}{4k_1\omega_{\min}^2} = \alpha_{\text{sat}}, \tag{21}$$

$$c = \frac{mg}{4k_1\omega_0^2} \ge \frac{mg}{4k_1\omega_{\max}^2} := c^\dagger \approx 0.05. \tag{22}$$

Inequality (21) always holds because $c \le \alpha_{\text{sat}}$. Then, it follows from (22) that if

$$c \ge c^\dagger,$$

then r^* could be zero by setting ω_0 as in (20). This result is illustrated by Fig. 3, when $c \ge c^\dagger$ (blue dotted curves), there exists ω_0 that could achieve $r^* = 0$.

4. Identification of uncontrollable modes

In this section, the controllable and uncontrollable modes are identified by conducting a controllability decomposition of the linearised system, and then a simple linear controller is presented for the quadcopter to track desired trajectories.

4.1. Linearized model

Define $\bar{\mathbf{x}} = \mathbf{x} - \mathbf{x}^*$ and $\bar{\mathbf{u}}_F = \mathbf{u}_F - \mathbf{u}_F^*$. Since $\dot{\mathbf{x}}^* = \mathbf{f}(\mathbf{x}^*, \mathbf{u}^*)$, it follows that

$$\begin{aligned}\dot{\bar{\mathbf{x}}} = \dot{\mathbf{x}} - \dot{\mathbf{x}}^* &= \mathbf{f}(\bar{\mathbf{x}} + \mathbf{x}^*, \bar{\mathbf{u}}_F + \mathbf{u}_F^*) - \dot{\mathbf{x}}^* \\ &\approx \mathbf{f}(\mathbf{x}^*, \mathbf{u}_F^*) + \mathbf{A}(\psi^*)\bar{\mathbf{x}} + \mathbf{B}\bar{\mathbf{u}}_F - \dot{\mathbf{x}}^* \\ &= \mathbf{A}(\psi^*)\bar{\mathbf{x}} + \mathbf{B}\bar{\mathbf{u}}_F \end{aligned} \tag{23}$$

where

$$\mathbf{A}(\psi^*) = \left.\frac{\partial \mathbf{F}(\bar{\mathbf{x}}, \bar{\mathbf{u}}_F)}{\partial \mathbf{x}}\right|_{\mathbf{x}=\mathbf{x}^*, \mathbf{u}_F=\mathbf{u}_F^*} = \begin{bmatrix} \mathbf{0}_{3\times3} & \mathbf{0}_{3\times3} & \mathbf{0}_{3\times3} & \mathbf{I}_{3\times3} \\ \mathbf{0}_{3\times3} & \mathbf{0}_{3\times3} & \mathbf{I}_{3\times3} & \mathbf{0}_{3\times3} \\ \mathbf{0}_{3\times3} & \mathbf{0}_{3\times3} & \mathbf{0}_{3\times3} & \mathbf{0}_{3\times3} \\ \mathbf{0}_{3\times3} & \mathbf{E}_{3\times3} & \mathbf{0}_{3\times3} & \mathbf{0}_{3\times3} \end{bmatrix} \in \mathbb{R}^{12\times12},$$

with $\mathbf{I}_{3\times3}$ as the identity matrix and

$$\mathbf{E}_{3\times3} = \begin{bmatrix} g\sin\psi^*(t) & g\cos\psi^*(t) & 0 \\ -g\cos\psi^*(t) & g\sin\psi^*(t) & 0 \\ 0 & 0 & 0 \end{bmatrix},$$

and

$$\mathbf{B} = \left.\frac{\partial \mathbf{F}(\bar{\mathbf{x}}, \bar{\mathbf{u}}_F)}{\partial \mathbf{u}_F}\right|_{\mathbf{x}=\mathbf{x}^*, \mathbf{u}_F=\mathbf{u}_F^*} = [\mathbf{0}_{3\times3}, \mathbf{0}_{3\times3}, \mathbf{Q}_{c1}^T, \mathbf{Q}_{c2}^T]^T \in \mathbb{R}^{12\times3}$$

where

$$\mathbf{Q}_{c1} = \begin{bmatrix} 0 & \frac{b_1 l}{I_x} & 0 \\ -\frac{b_1 l}{I_y} & 0 & \frac{b_1 l}{I_y} \\ \frac{n_2 l}{I_z} & -\frac{n_3 l}{I_z} & \frac{n_4 l}{I_z} \end{bmatrix}, \mathbf{Q}_{c2} = \begin{bmatrix} 0 & 0 & 0 \\ 0 & 0 & 0 \\ \frac{b_1}{m} & \frac{b_1}{m} & \frac{b_1}{m} \end{bmatrix},$$

and $n_i = 2\alpha_i^* b_3 + b_4$.

4.2. Controllability analysis

The controllability matrix $\mathbf{Q}_c$ of system (23) is

$$\mathbf{Q}_c = \begin{bmatrix}\mathbf{B} & \mathbf{AB} & \mathbf{A}^2\mathbf{B} & \dots & \mathbf{A}^{11}\mathbf{B}\end{bmatrix} = \begin{bmatrix} \mathbf{0}_{3\times3} & \mathbf{Q}_{c2} & \mathbf{0}_{3\times3} & \mathbf{Q}_{c3} & \\ \mathbf{0}_{3\times3} & \mathbf{Q}_{c1} & \mathbf{0}_{3\times3} & \mathbf{0}_{3\times3} & \mathbf{0}_{12\times24} \\ \mathbf{Q}_{c1} & \mathbf{0}_{3\times3} & \mathbf{0}_{3\times3} & \mathbf{0}_{3\times3} & \\ \mathbf{Q}_{c2} & \mathbf{0}_{3\times3} & \mathbf{Q}_{c3} & \mathbf{0}_{3\times3} & \end{bmatrix} \in \mathbb{R}^{12\times36},$$

where

$$\mathbf{Q}_{c3} = \begin{bmatrix} -\frac{P_c}{I_y} & \frac{P_s}{I_x} & \frac{P_c}{I_y} \\ -\frac{P_s}{I_y} & -\frac{P_c}{I_x} & \frac{P_s}{I_y} \\ 0 & 0 & 0 \end{bmatrix},$$

$$P_c = b_1 lg\cos\psi^*(t), \quad P_s = b_1 lg\sin\psi^*(t).$$

Matrix $\mathbf{Q}_c$ is sparse and highly structured. It can be verified that $\text{rank}(\mathbf{Q}_c) = 10$ when the rated speed $\omega_0 > 0$. Since there are 12 states, we know that two modes are uncontrollable.

To further identify the uncontrollable modes, we conduct a controllability decomposition as follows. Following [24,25], we design

$$\mathbf{T} = \begin{bmatrix} \mathbf{0}_{3\times3} & \mathbf{Q}_{c2} & \mathbf{0}_{3\times2} & \mathbf{Q}_{c4} & \mathbf{0}_{3\times2} \\ \mathbf{0}_{3\times3} & \mathbf{Q}_{c1} & \mathbf{0}_{3\times2} & \mathbf{0}_{3\times2} & \mathbf{Q}_{c5} \\ \mathbf{Q}_{c1} & \mathbf{0}_{3\times3} & \mathbf{0}_{3\times2} & \mathbf{0}_{3\times2} & \mathbf{Q}_{c6} \\ \mathbf{Q}_{c2} & \mathbf{0}_{3\times3} & \mathbf{Q}_{c4} & \mathbf{0}_{3\times2} & \mathbf{0}_{3\times2} \end{bmatrix},$$

$$\mathbf{Q}_{c4} = \begin{bmatrix} -\frac{P_c}{I_y} & \frac{P_s}{I_x} \\ -\frac{P_s}{I_y} & -\frac{P_c}{I_x} \\ 0 & 0 \end{bmatrix},$$

$$\mathbf{Q}_{c5} = \begin{bmatrix} 0 & 0 \\ 0 & 0 \\ 0 & 1 \end{bmatrix}, \mathbf{Q}_{c6} = \begin{bmatrix} 0 & 0 \\ 0 & 0 \\ 1 & 0 \end{bmatrix},$$

where $\mathbf{T} \in \mathbb{R}^{12\times12}$ is invertible. Then we define

$$\tilde{\mathbf{x}} = \mathbf{T}^{-1}\bar{\mathbf{x}}. \tag{24}$$

Substituting (24) into (23) leads to $\dot{\tilde{\mathbf{x}}} = \mathbf{T}^{-1}\mathbf{AT}\tilde{\mathbf{x}} + \mathbf{T}^{-1}\mathbf{B}\bar{\mathbf{u}}_F$. Let $\tilde{\mathbf{A}} = \mathbf{T}^{-1}\mathbf{AT}$ and $\tilde{\mathbf{B}} = \mathbf{T}^{-1}\mathbf{B}$. Then, it follows that $\dot{\tilde{\mathbf{x}}} = \tilde{\mathbf{A}}\tilde{\mathbf{x}} + \tilde{\mathbf{B}}\bar{\mathbf{u}}_F$, whose sub-block matrix form is

$$\begin{bmatrix} \dot{\tilde{\mathbf{x}}}_c \\ \dot{\tilde{\mathbf{x}}}_{\bar{c}} \end{bmatrix} = \begin{bmatrix} \tilde{\mathbf{A}}_c & \tilde{\mathbf{A}}_{12} \\ \mathbf{0}_{2\times10} & \tilde{\mathbf{A}}_{\bar{c}} \end{bmatrix} \begin{bmatrix} \tilde{\mathbf{x}}_c \\ \tilde{\mathbf{x}}_{\bar{c}} \end{bmatrix} + \begin{bmatrix} \tilde{\mathbf{B}}_c \\ \mathbf{0}_{2\times3} \end{bmatrix} \bar{\mathbf{u}}_F, \tag{25}$$

where

$$\tilde{\mathbf{A}}_c = \begin{bmatrix} \mathbf{0}_{3\times3} & \mathbf{0}_{3\times3} & \mathbf{0}_{3\times2} & \mathbf{0}_{3\times2} \\ \mathbf{I}_{3\times3} & \mathbf{0}_{3\times3} & \mathbf{0}_{3\times2} & \mathbf{0}_{3\times2} \\ \mathbf{0}_{2\times3} & \mathbf{H}_{2\times3} & \mathbf{0}_{2\times2} & \mathbf{0}_{2\times2} \\ \mathbf{0}_{2\times3} & \mathbf{0}_{2\times3} & \mathbf{I}_{2\times2} & \mathbf{0}_{2\times2} \end{bmatrix},$$

$$\mathbf{H}_{2\times3} = \begin{bmatrix} 1 & 0 & -1 \\ 0 & 1 & 0 \end{bmatrix}, \quad \tilde{\mathbf{A}}_{12} = \mathbf{0}_{10\times2},$$

$$\tilde{\mathbf{A}}_{\bar{c}} = \begin{bmatrix} 0 & 0 \\ 1 & 0 \end{bmatrix}, \quad \tilde{\mathbf{B}}_c = \begin{bmatrix} \mathbf{I}_{3\times3} \\ \mathbf{0}_{3\times3} \\ \mathbf{0}_{2\times3} \\ \mathbf{0}_{2\times3} \end{bmatrix}.$$

Equation (25) shows that the system is decomposed into an uncontrollable subsystem $\dot{\tilde{\mathbf{x}}}_{\bar{c}} = \tilde{\mathbf{A}}_{\bar{c}}\tilde{\mathbf{x}}_{\bar{c}}$ and a controllable subsystem $\dot{\tilde{\mathbf{x}}}_c = \tilde{\mathbf{A}}_c\tilde{\mathbf{x}}_c + \tilde{\mathbf{A}}_{12}\tilde{\mathbf{x}}_{\bar{c}} + \tilde{\mathbf{B}}_c\bar{\mathbf{u}}_F$. The transformed states are

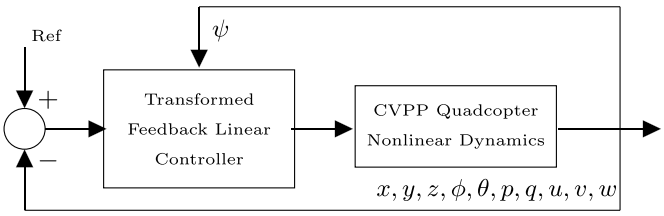

Fig. 4. Block diagram of the CVPP quadcopter control scheme.

$$\begin{bmatrix} \tilde{\mathbf{x}}_c \\ \tilde{\mathbf{x}}_{\bar{c}} \end{bmatrix} = \mathbf{T}^{-1}\bar{\mathbf{x}} = \begin{bmatrix} \frac{mx_{12}}{2b_1} - \frac{I_x x_7}{2lb_1} - \frac{I_y x_8}{2lb_1} \\ \frac{I_x x_7}{lb_1} \\ \frac{mx_{12}}{2b_1} - \frac{I_x x_7}{2lb_1} + \frac{I_y x_8}{2lb_1} \\ \frac{mx_3}{2b_1} - \frac{I_x x_4}{2lb_1} - \frac{I_y x_5}{2lb_1} \\ \frac{I_x x_4}{lb_1} \\ \frac{mx_3}{2b_1} - \frac{I_x x_4}{2lb_1} + \frac{I_y x_5}{2lb_1} \\ -\frac{I_y(x_{10}\cos\psi^* + x_{11}\sin\psi^*)}{lb_1 g} \\ -\frac{I_x(x_{11}\cos\psi^* - x_{10}\sin\psi^*)}{lb_1 g} \\ -\frac{I_y(x_1\cos\psi^* + x_2\sin\psi^*)}{lb_1 g} \\ -\frac{I_x(x_2\cos\psi^* - x_1\sin\psi^*)}{lb_1 g} \\ x_9 + x_{12}k_{\bar{c}_1} - x_8 k_{\bar{c}_2} + x_7 k_{\bar{c}_3} \\ x_6 + x_3 k_{\bar{c}_1} - x_5 k_{\bar{c}_2} + x_4 k_{\bar{c}_3} \end{bmatrix}, \tag{26}$$

$$k_{\bar{c}_1} = \frac{ml(n_2 - n_4)}{2I_z b_1}, \; k_{\bar{c}_2} = \frac{I_y(n_2 + n_4)}{2I_z b_1},$$

$$k_{\bar{c}_3} = \frac{I_x(2n_3 - n_2 + n_4)}{2I_z b_1},$$

where x_i (i ranges from 1 to 12) are the elements of $\bar{\mathbf{x}}$, and $\tilde{\mathbf{x}}_c$ and $\tilde{\mathbf{x}}_{\bar{c}}$ are controllable and uncontrollable modes, respectively.

As can be seen from (26), the uncontrollable states in $\tilde{\mathbf{x}}_{\bar{c}}$, which correspond to the last two elements of the vector, contain x_9 and x_6 that correspond to r and ψ, respectively. As a result, the yaw angle and its angular rate are uncontrollable.

4.3. A linear controller

Fig. 4 shows a block diagram of the control scheme for a faulty CVPP quadcopter. Based on the decomposed controllable system (25), a linear state feedback controller can be designed. Consider a simple feedback design H_∞ controller is presented to enhance the robustness of the system. Other control methods like LQG could also be used. According to the faulty system (25), the H_∞ controller is designed as

$$\begin{aligned} \dot{\tilde{\mathbf{x}}} &= \tilde{\mathbf{A}}\tilde{\mathbf{x}} + \tilde{\mathbf{B}}_1\mathbf{w} + \tilde{\mathbf{B}}_2\mathbf{u}, \\ \mathbf{z}_\infty &= \tilde{\mathbf{C}}_1\tilde{\mathbf{x}} + \mathbf{D}_{12}\mathbf{u}, \\ \tilde{\mathbf{y}} &= \tilde{\mathbf{C}}_2\tilde{\mathbf{x}}, \end{aligned} \tag{27}$$

where

$$\tilde{\mathbf{A}} = \begin{bmatrix} \mathbf{0}_{3\times3} & \mathbf{0}_{3\times3} & \mathbf{0}_{3\times2} & \mathbf{0}_{3\times2} \\ \mathbf{I}_{3\times3} & \mathbf{0}_{3\times3} & \mathbf{0}_{3\times2} & \mathbf{0}_{3\times2} \\ \mathbf{0}_{2\times3} & \mathbf{H}_{2\times3} & \mathbf{0}_{2\times2} & \mathbf{0}_{2\times2} \\ \mathbf{0}_{2\times3} & \mathbf{0}_{2\times3} & \mathbf{I}_{2\times2} & \mathbf{0}_{2\times2} \end{bmatrix},$$

$$\tilde{\mathbf{B}}_1 = \begin{bmatrix} \mathbf{I}_{3\times3} \\ \mathbf{0}_{3\times3} \\ \mathbf{0}_{2\times3} \\ \mathbf{0}_{2\times3} \end{bmatrix}, \quad \tilde{\mathbf{B}}_2 = \begin{bmatrix} \mathbf{I}_{3\times3} \\ \mathbf{0}_{3\times3} \\ \mathbf{0}_{2\times3} \\ \mathbf{0}_{2\times3} \end{bmatrix},$$

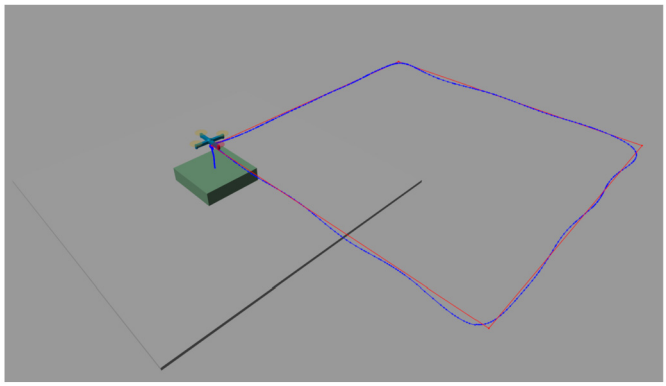

Fig. 5. Trajectory tracking results. The blue dotted curves represent the actual flying trajectory and the red line is the reference square trajectory with 10 m length on each side. The faulty propeller is highlighted in red.

$$\tilde{\mathbf{C}}_2 = \begin{bmatrix} \mathbf{0}_{3\times3} & \mathbf{Q}_{c2} & \mathbf{0}_{3\times2} & \mathbf{Q}_{c4} \\ \mathbf{0}_{2\times3} & \mathbf{S} & \mathbf{0}_{2\times2} & \mathbf{0}_{2\times2} \\ \mathbf{S} & \mathbf{0}_{2\times3} & \mathbf{0}_{2\times2} & \mathbf{0}_{2\times2} \\ \mathbf{Q}_{c2} & \mathbf{0}_{3\times3} & \mathbf{Q}_{c4} & \mathbf{0}_{3\times2} \end{bmatrix},$$

$$\tilde{\mathbf{C}}_1 = \begin{bmatrix} I_{10\times10} \\ \mathbf{0}_{3\times10} \end{bmatrix}, \quad \mathbf{D}_{12} = \begin{bmatrix} \mathbf{0}_{10\times3} \\ I_{3\times3} \end{bmatrix},$$

$$\mathbf{S} = \begin{bmatrix} 0 & \frac{b_1 l}{I_x} & 0 \\ -\frac{b_1 l}{I_y} & 0 & \frac{b_1 l}{I_y} \end{bmatrix}.$$

It can be found in (27) that, $\tilde{\mathbf{x}}$ is the decomposed state, $\mathbf{w}$ is the disturbance, $\mathbf{u}$ represents the control signal, and $\mathbf{z}_\infty$ is the error value that needs to be minimized.

5. Simulation validation

This section presents two simulation experiments to verify the theoretical findings. The simulation is conducted in a physical environment built in Simscape in Matlab. It combines detailed physical component models based on first principles. The parameter values are shown in Table 1. A low pass filter with a 10 Hz cut-off frequency is used to represent the dynamics of the propeller actuator. The input of the low pass filter is the expected value of the pitch angle and the output is the response value. Noise with 20 dB signal-to-noise ratio is added to all states as measurement noise.

In the first experiment, it is assumed that the propeller 1 has malfunctioned from the beginning with a fixed pitch angle of 0.18 rad and a spinning speed of 707.7 rad/s. Moreover, we assume that these values can be measured and used by the controller. The quadcopter is required to track a trajectory simulating taking off, moving along a square trajectory with 10 m length on each side, and landing, shown in Fig. 5.

The results are shown in Fig. 6. As can be seen, although the yaw angle and its rate are uncontrollable, a CVPP quadcopter with a faulty actuator is still able to accurately track the desired position trajectory and the value of r remains close to zero, which is consistent with our analysis.

In the second experiment, the performance of the proposed controller given a variety of initial conditions is examined. The initial state is $[x_0, y_0, z_0, \phi_0, \theta_0] = [0, 0, 0, \phi_r, \theta_r]$ and the target state is $[x^*, y^*, z^*, \phi^*, \theta^*] = [0, 0, 0, 0, 0]$, where the values of ϕ_r and θ_r are generated randomly from a uniform distribution in [-1.57,1.57] rad. Assume the quadcopter VPP 1 stuck at 0.05 rad and a spinning speed of 996.9 rad/s. When the state gets sufficiently close to the target state after 5 s, the quadcopter is regarded as stable; otherwise it is unstable.

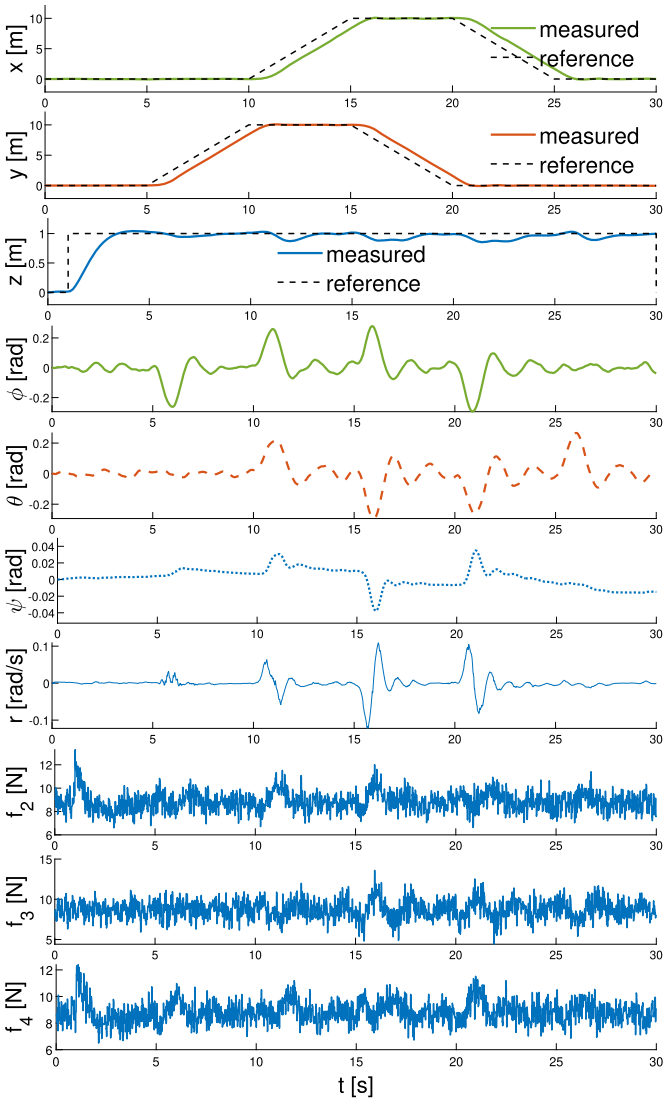

Fig. 6. Simulation results of a CVPP quadcopter subject to propeller faults. The trajectory is shown in black dot lines. The yaw angle ψ and angular rate r are uncontrollable but approach the theoretical prediction.

We conducted 100 trails, each with a different initial condition (ϕ_r and θ_r). Fig. 7 shows that the controller works well under a wide range of initial conditions, with a success rate of 95 percent. It is shown that the quadcopter does not cope well when both pitch (θ) and roll (ϕ) are large negative angles. Fig. 8 shows the results of a typical simulation trail, demonstrating the control law to work well.

6. Conclusion

In this paper, the dynamics and control of CVPP quadcopters in the presence of a faulty propeller is studied, that is, a propeller that can no longer adjust its pitch angle. The equilibrium trajectory was analysed from the beginning in this paper, the uncontrollable modes were identified next, and a linear controller was proposed at last. The correlation between the self-rotation speed and the common propeller spinning rate was characterized. The specific condition under which a faulty CVPP quadcopter could hover steadily without self-rotation was given. We believe the new findings could further enhance the development for CVPP quadcopters for high-performance flights in the future. The findings were further validated by physics-based simulation experiments.

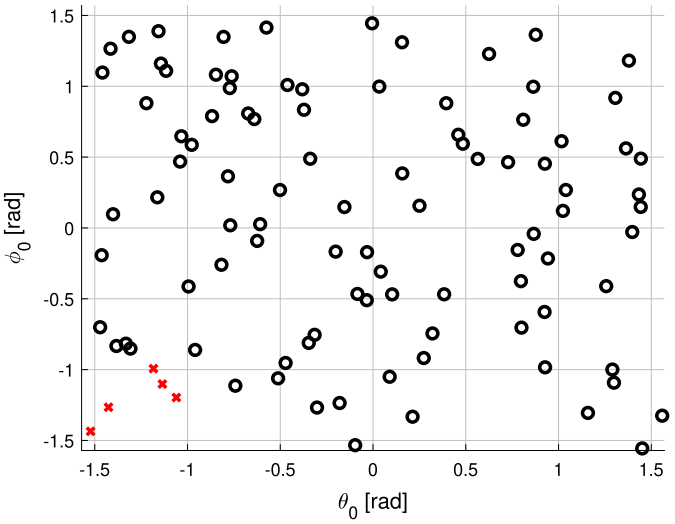

Fig. 7. Results from physics-based simulations for 100 random initial states. The x-axis and y-axis show the initial pitch (θ_0) and roll (ϕ_0) angles respectively. A black circle indicates that the faulty quadcopter achieved stability, whereas the red cross indicates that it lost stability.

In this work, fault detection or isolation was not considered, which is, however, important for future research. The properties of CVPP quadcopters in the presence of two or three faulty propellers and other types of faults will be explored.

Declaration of competing interest

The authors declare that they have no known competing financial interests or personal relationships that could have appeared to influence the work reported in this paper.

References

[1] C.A. Wargo, G.C. Church, J. Glaneueski, M. Strout, Unmanned aircraft systems (UAS) research and future analysis, in: Proceedings of 2014 IEEE Aerospace Conference, IEEE, 2014, pp. 1–16.

[2] G. Skorobogatov, C. Barrado, E. Salamí, Multiple UAV systems: a survey, Unmanned Syst. 8 (02) (2020) 149–169.

[3] A. Mohiuddin, T. Tarek, Y. Zweiri, D. Gan, A survey of single and multi-UAV aerial manipulation, Unmanned Syst. 8 (02) (2020) 119–147.

[4] A. Devos, E. Ebeid, P. Manoonpong, Development of autonomous drones for adaptive obstacle avoidance in real world environments, in: Proceedings of 2018 21st Euromicro Conference on Digital System Design (DSD), 2018, pp. 707–710.

[5] Z. Yu, Y. Zhang, B. Jiang, C.Y. Su, J. Fu, Y. Jin, T. Chai, Decentralized fractional-order backstepping fault-tolerant control of multi-UAVs against actuator faults and wind effects, Aerosp. Sci. Technol. 104 (2020) 105939.

[6] S. Xu, H. Wen, Z. Huang, Robust fuzzy sampled-data attitude control of spacecraft with actuator saturation and persistent disturbance, Aerosp. Sci. Technol. 101 (2020) 105850.

[7] S. Allison, H. Bai, B. Jayaraman, Wind estimation using quadcopter motion: a machine learning approach, Aerosp. Sci. Technol. 98 (2020) 105699.

[8] N. Gupta, M. Kothari Abhishek, Flight dynamics and nonlinear control design for variable-pitch quadrotors, in: Proceedings of 2016 American Control Conference (ACC), IEEE, 2016, pp. 3150–3155.

[9] M. Cutler, J. How, Actuator constrained trajectory generation and control for variable-pitch quadrotors, in: Proceedings of AIAA Guidance, Navigation, and Control Conference, 2012, pp. 4777–4792.

[10] M.W. Mueller, R. D'Andrea, Relaxed hover solutions for multicopters: application to algorithmic redundancy and novel vehicles, Int. J. Robot. Res. 35 (8) (2016) 873–889.

[11] A.F.S.l. Alessandro Baldini, Riccardo Felicetti, A. Monteriù, Actuator fault tolerant control of variable pitch quadrotor vehicles, in: Proceedings of 2021 21st IFAC World Congress, IFAC, 2020.

[12] M. Tahavori, A. Hasan, Fault recoverability for nonlinear systems with application to fault tolerant control of UAVs, Aerosp. Sci. Technol. 107 (2020) 106282.

[13] R.C. Avram, X. Zhang, J. Muse, Nonlinear adaptive fault-tolerant quadrotor altitude and attitude tracking with multiple actuator faults, IEEE Trans. Control Syst. Technol. 26 (2) (2018) 701–707.

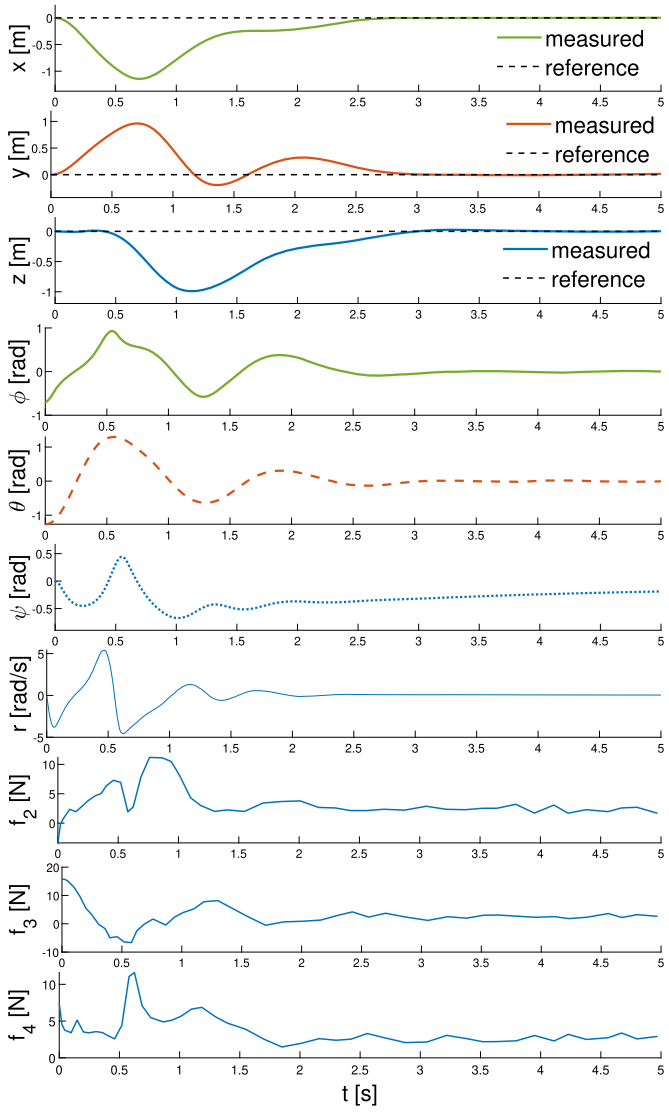

Fig. 8. Simulation results of random initial angle scenario where the initial state is $[x, y, z, \phi, \theta] = [0, 0, 0, -0.7, -1.26]$ and the target state is $[x^*, y^*, z^*, \phi^*, \theta^*] = [0, 0, 0, 0, 0]$.

[14] Z. Liu, C. Yuan, Y. Zhang, J. Luo, A learning-based fault tolerant tracking control of an unmanned quadrotor helicopter, J. Intell. Robot. Syst. 84 (1–4) (2016) 145–162.

[15] Z. Hou, P. Lu, Z. Tu, Nonsingular terminal sliding mode control for a quadrotor UAV with a total rotor failure, Aerosp. Sci. Technol. 98 (2020) 105716.

[16] Z. Wang, R. Groß, S. Zhao, Controllability analysis and controller design for variable-pitch propeller quadcopters with one propeller failure, Advanced Control for Applications: Engineering and Industrial Systems (2020) e29 (Invited special issue).

[17] S. Sheng, C. Sun, Control and optimization of a variable-pitch quadrotor with minimum power consumption, Energies 9 (4) (2016) 232–249.

[18] T. Pang, K. Peng, F. Lin, B.M. Chen, Towards long-endurance flight: design and implementation of a variable-pitch gasoline-engine quadrotor, in: Proceedings of 2016 12th IEEE International Conference on Control and Automation (ICCA), IEEE, 2016, pp. 767–772.

[19] E. Gopalakrishnan, Quadcopter flight mechanics model and control algorithms, Masters' Thesis, Department of Control Engineering, Lulea University of Technology, Czech Technical University, Prague, Czechia, 2017.

[20] A. Letalenet, P. Morin, Identification and evaluation of a force model for multi-rotor uavs, in: 2020 IEEE International Conference on Robotics and Automation (ICRA), IEEE, 2020, pp. 4280–4286.

[21] G.P. Rible, A.A. Nicolette, R. Manuel, Modeling and implementation of quadcopter autonomous flight based on alternative methods to determine propeller parameters, Adv. Sci. Technol. Eng. Syst. J. 5 (5) (2020) 727–741.

[22] A. Freddi, A. Lanzon, S. Longhi, A feedback linearization approach to fault tolerance in quadrotor vehicles, IFAC Proc. Vol. 44 (1) (2011) 5413–5418.

[23] M. Cutler, J.P. How, Analysis and control of a variable-pitch quadrotor for agile flight, J. Dyn. Syst. Meas. Control 137 (10) (2015) 101002–101016.
[24] D. Boley, Computing the Kalman decomposition: an optimal method, IEEE Trans. Autom. Control 29 (1) (1984) 51–53.
[25] M. Petreczky, R. Tóth, G. Mercère, Realization theory for LPV state-space representations with affine dependence, IEEE Trans. Autom. Control 62 (9) (2016) 4667–4674.